Biosensors and Bioelectronics 68 (2015) 288–294

Contents lists available at ScienceDirect

Biosensors and Bioelectronics

journal homepage: www.elsevier.com/locate/bios

Efficient immobilization of acetylcholinesterase onto amino functionalized carbon nanotubes for the fabrication of high sensitive organophosphorus pesticides biosensors

Guangxia Yu [a,b], Weixiang Wu [a,b], Qiang Zhao [a,b], Xiaoyun Wei [a,b], Qing Lu [a,b,*]

[a] Key Laboratory of Environment and Health, Ministry of Education & Ministry of Environmental Protection, School of Public Health, Tongji Medical College, Huazhong University of Science and Technology, #13 Hangkong Road, Wuhan, Hubei, 430030, China
[b] State Key Laboratory of Environmental Health (Incubating), School of Public Health, Tongji Medical College, Huazhong University of Science and Technology, #13 Hangkong Road, Wuhan, Hubei, 430030, China

ARTICLE INFO

Article history:
Received 21 October 2014
Received in revised form
15 December 2014
Accepted 2 January 2015
Available online 3 January 2015

Keywords:
Organophosphorus pesticide biosensor
Surface functionalization
Carbon nanotubes
Protein adsorption
Orientation
Paraoxon

ABSTRACT

This work introduced an efficient immobilization of acetylcholinesterase (AChE) onto amino functionalized carbon nanotubes (CNT–NH_2), in order to fabricate high sensitive and practical organophosphorus pesticide (OPs) biosensors. Compared with the pristine, –COOH and –OH decorated CNTs, there were larger amount of enzymes adsorbed on the surface of CNT–NH_2 with a favorable orientation and the best amperometric response was obtained on the AChE/CNT–NH_2/GC electrode. Furthermore, the biosensor modified with CNT–NH_2 showed a high affinity to acetylthiocholine chloride (ATCh) and could catalyze the hydrolysis of ATCh with an apparent Michaelis–Menten constant (K_m) value of 67.4 μM. Using paraoxon as a model compound, wide linear ranges from 0.2 nM to 1 nM and 1 nM to 30 nM, and a low detection limit of 0.08 nM were obtained with satisfactory reproducibility and stability. Moreover, the biosensor had also been successfully employed for the determination of low concentrations of pesticides in real vegetable samples. This method could be extended to other functionalized nano–materials for their application in constructing biosensors.

1. Introduction

Efficient immobilization of the enzyme onto the electrode surface while maintaining its native catalytic activity is the key consideration to develop ultrasensitive enzyme based biosensors. Ideally, it is expected that enzymes can be bound to the electrode surface with a favorable orientation while avoiding conformational changes (Ganesana et al., 2011). The existing immobilization methods include direct physical adsorption (Sotiropoulou et al., 2005), physical entrapment in polymers or sol–gels (Dutta and Puzari, 2014; Zou et al., 2008), cross linking (Lai et al., 2009), covalent attachment (Zhang et al., 2005) and self assembling (Liu and Lin, 2006). However, the enzyme immobilizations with these approaches are hard to control, because as contributions of either hydrophobic interactions, hydrogen bonding or electrostatic attraction, the main driving forces of protein–particle interactions are often not fully enlightened (Meder et al., 2013a). Moreover, these traditional methods usually need complicated steps, leading them to hardly satisfy the requirement of practical applications.

In recent years, surface functionalization, which allows tailoring the surface properties of nano-materials, has been applied to investigate the interaction between protein and particle surface. Numerous researches had demonstrated that specific design of nano–materails by surface functionalization tailored with charge groups (like –COOH, –NH_2, –SO_3H, etc.) might be a tool to control driving forces of proteins adsorption and orientation (Meder et al., 2013a, 2013b). Moreover, certain surface chemistries even feature protein adsorption comparable to antigen–antibody interactions (Hoshino et al., 2010; Monopoli et al., 2012). Meder et al. (2012) had discussed the interaction between the surface of colloidal alumina (Al_2O_3) particles decorated with different functional groups (–NH_2, –COOH, –SO_3H and –PO_3H_2) and three model proteins, bovine serum albumin (BSA), lysozyme (LSZ) and trypsin (TRY). It had been demonstrated that BSA was preferentially adsorbed on the positively charged surfaces of Al_2O_3 and Al_2O_3–NH_2, while LSZ and TRY were adsorbed on negatively charged Al_2O_3–COOH, Al_2O_3–SO_3H and Al_2O_3–PO_3H_2. Furthermore, the regions in

* Corresponding author at: School of Public Health, Tongji Medical College, Huazhong University of Science and Technology, #13 Hangkong Road, Wuhan, Hubei 430030, China. Fax: +86 27 83657765.
E-mail address: qi_weiliao@126.com (Q. Lu).

http://dx.doi.org/10.1016/j.bios.2015.01.005
0956-5663/

protein with dominant positive or negative potential could be the adsorption sites on oppositely charged particle surfaces, indicating that the protein oriented adsorption was influenced by the type of functional groups via electrostatic interactions as driven forces. Gessner et al. (2003) had discussed the influences of different basic and acidic function groups on the surface of polystyrene on the protein adsorption. The studies had shown that proteins with isoelectric point pI > 5.5 preferred to bind acidic functional groups in neutral or subalkalic experiment conditions and vice versa. A conclusion could be drawn that the adsorption should be mainly driven by Coulomb forces. These researches above had provided a prerequisite for the design of functionally graded materials to realize the protein oriented adsorptions, thus we put forward a hypothesis that chemical functionalized nano-materials could also be employed to control the immobilization of enzymes onto the electrode surface without any other cross–linking agent.

Carbon nanotubes (CNTs) have been extensively used for the development of biosensors as electronic bridges and signal amplifiers due to their superior electrical conductivity, high electrochemical catalytic activity, biocompatibility and nontoxicity (Kim et al., 2007). Additionally, CNTs have excellent electrocatalytic activity for thiocholine (Liu et al., 2005), the product enzymatically generated by AChE, which could provide a prerequisite for the construction of AChE based OPs biosensors. As is reported, the isoelectric point of AChE from electric eel is 5.5, thus the net surface charge of AChE is negative in neutral or subalkalic experiment conditions (Choi et al., 2001). Furthermore, the active-site gorge region of AChE had been investigated to be negatively charged (Dvir et al., 2010; Ripoll et al., 1993), thus it could work as an adsorption site bonding to the positively charged nano-materials. Thereby, in this work, we applied the positively charged CNT–NH_2 as a model to demonstrate an efficient immobilization of AChE for the fabrication of high sensitive and practical OPs biosensors.

In this system, amino functionalized CNTs, in addition to serving as electronic bridges and signal amplifiers, could also be a tool to control the efficient immobilization of enzymes. The advantages of this method were as follows: (1) guiding the protein orientation and reducing randomly bounded proteins, therefore improving the sensitivity; (2) improving the affinity between the enzyme and nano-materials, thus promoting the electron transfer mechanism between enzyme and electrode; (3) simplifying the immobilization steps, thus improving the reproducibility and operability. The proposed method could be further applied as a common approach for the design of various biosensors with functionalized materials.

2. Experimental

2.1. Reagents

Acetylthiocholine chloride (ATCh) and acetylcholinesterase (1000 Units/mg, from electric eel) were obtained from Sigma-Aldrich (St. Louis, MO). Multiwalled carbon nanotubes (purity > 95%) were purchased from the Chengdu Organic Chemistry Institute (Chengdu China) and the 3–aminopropyltriethoxysilane (3–APTES) was purchased from Aladdin Industrial Corporation (Shanghai China). The standard sample of paraoxon was obtained from the Future of Shanghai Industrial Co., Ltd. (Shanghai China). Practical vegetable samples were purchased from the local market. All the other reagents were of analytical grade. All aqueous solutions were prepared with doubly distilled water.

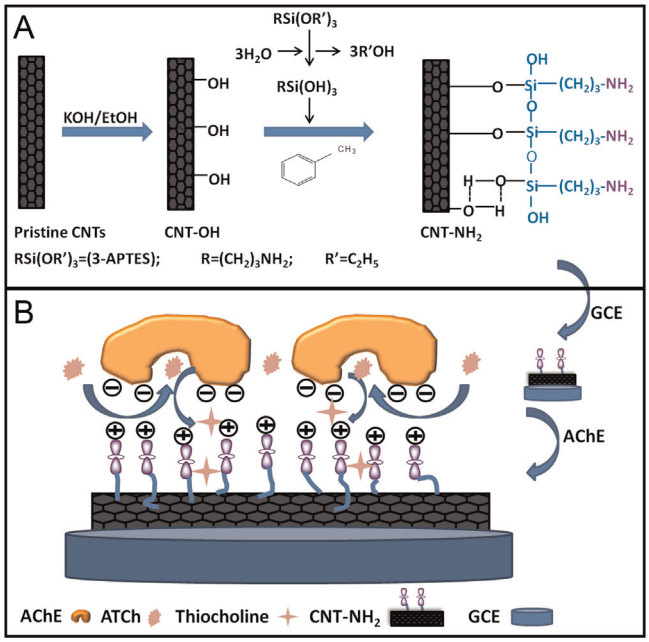

Fig. 1. (A) Schematic representation of amination process of carbon nanotubes; (B) schematic representation of the efficient immobilization of AChE onto the CNT–NH_2 modified electrode.

2.2. Apparatus

Electrochemical measurements were carried out using a conventional three-electrode system. A bare or modified glass carbon electrode was served as working electrode, a standard calomel electrode (SCE) as reference electrode and a platinum wire as counter electrode. Impedance–Time Parameters (current–time) and Differential Pulse Voltammetry (DPV) were performed on a CHI830C electrochemical workstation (Shanghai Chenhua Apparatus, China). Electrochemical impedance spectroscopy (EIS) was worked at a CHI660C electrochemical workstation (Shanghai Chenhua Apparatus, China). Infrared spectrometry (IR) (VERTEX 70, Bruker, Germany) and X-ray photoelectron spectroscopy (XPS, AXIS-ULTRA DLD-600W, SHIMADZU, Japan) were applied to characterize the functionalized CNTs. The gas chromatography (GC) analysis was conducted on an Agilent 7890A (the USA). The amount of adsorbed protein was detected with a UV spectrophotometer (UV–1800, SHIMADZU, Japan).

2.3. Surface functionalization of CNTs

The surface amination of CNTs was carried out by the procedures described by Song et al. (Song et al., 2009). A schematic representation of the amination processes was shown in Fig. 1A. Firstly, 100 mg pristine CNTs were mixed with 100 mL ethyl alcohol (EtOH) and 5 g KOH, and then refluxed for 8 h, followed by the filtration and washing process with ethanol and doubly distilled water to obtain CNT–OH. Secondly, 50 mg CNT–OH was dispersed in toluene via sonication for 30 min and then an excess of 3–APTES solution was added drop by drop to obtain the produced mixture which should be stirred at 80 °C for 8 h. The tubes were then rinsed with toluene and ethanol, dried at 80 °C and finally designated as CNT–NH_2. Besides, CNT–COOH was obtained by acid treatment with H_2SO_4:HNO_3 (1:3) (Tzavalas et al., 2006).

2.4. Preparation of OPs biosensors

Schematic illustration of the enzyme immobilization onto electrode surface was shown in Fig. 1B. Firstly, 5 μL 0.5 mg/mL

$CNT–NH_2$ suspensions ($CNT–NH_2$) were placed onto the surface of polished GCEs and allowed air-dry at room temperature. After the water was evaporated, the modified GCEs were coated with 5 μL 0.02 mg/mL AChE, which was prepared with 0.1 M pH 8.0 phosphate buffer solutions (PBS). Then the AChE/$CNT–NH_2$/GCE was obtained after being dried at room temperature. Meanwhile, in order to discuss the influence of different functional groups during the immobilization of enzymes, the AChE/pristine CNTs/GCE, AChE/CNT–OH/GCE and AChE/CNT–COOH/GCE were fabricated in the same way. Before use, the electrodes were soaked in a stirred solution of 0.1 M PBS for about 10 min in order to remove loosely bound enzymes and CNTs from the GCE. The prepared biosensors were stored at 4 °C when not in use.

2.5. Protein adsorption

The amount of adsorbed enzyme on different functionalized CNTs was studied. CNTs suspensions were prepared by sonicating the mixture of 5 mg (accurate to 0.01 mg) of $CNT–NH_2$, CNT–COOH, CNT–OH and pristine CNTs with 5 mL pH 8.0 PBS (corresponding to a 1 mg/mL suspension) for 30 min. Then 50 μL accurately prepared AChE solution (1 mg/mL) was added to 50 μL CNTs suspensions. After the mixing process, let the solution stand for 3 h at 25 °C. The concentrations of unbound proteins were determined in the supernatant by measuring UV light absorption at 280 nm in a UV spectrophotometer after separating CNTs–protein conjugates by centrifugation for 10 min at 12000 rpm. The amount of the adsorbed protein was calculated by figuring the difference of the concentration between the samples with and without CNTs.

2.6. Preparation and determination of real samples

Vegetable samples (cabbage, celery, onion, carrot) were obtained from the local markets. Fifteen gram of each sample was homogenized and extracted with 80 mL of acetone with stirring for 0.5 h. Then the supernatants were taken and filtered through a 0.45 μm membrane and finally evaporated to dryness. After that, 5 mL dichloromethane was added to the dry residue. The standard adding method was also applied to control the analytical quality according to the procedure described by Li et al. (2006). In short, the cabbage, onion and carrot were sprayed with 5 nM paraoxon stock solution and stored at 4 °C for 24 h. After that, 15 g of each sample was chopped and extracted with acetone. The rest of the steps were similar to the procedures mentioned above. After the pretreatment, the acquired solution was detected by the biosensor and GC method (GBT 5009.20–2003) directly. The concentration of

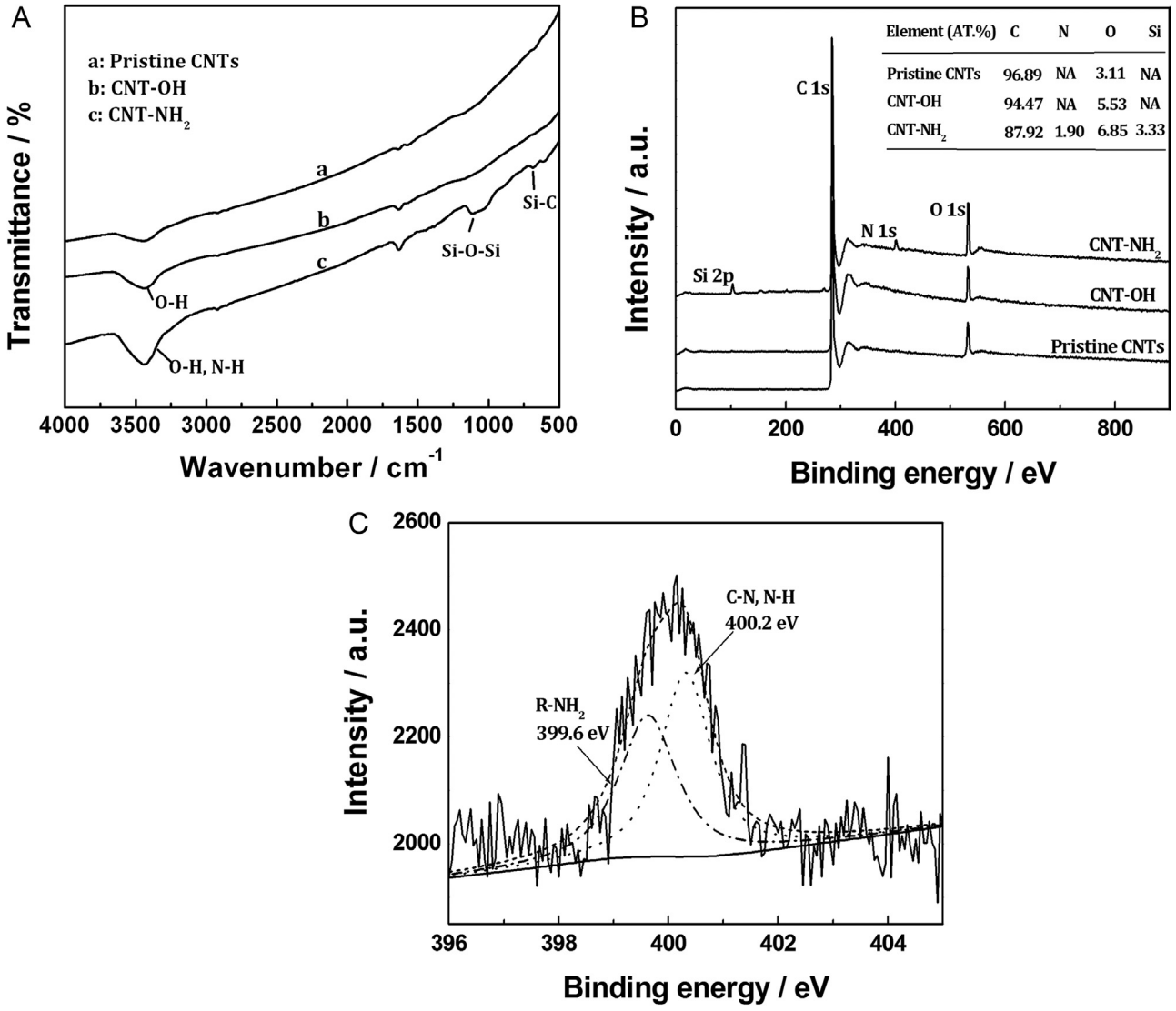

Fig. 2. (A) IR spectra of (a) pristine CNTs, (b) CNT–OH and (c) $CNT–NH_2$; (B) XPS spectra of pristine CNTs, CNT–OH and $CNT–NH_2$; (C) N 1 s spectra of $CNT–NH_2$.

pesticides in the samples could be obtained from the calibration curve.

3. Results and discussion

3.1. Characterization of functionalized CNTs

Infrared spectrometry was exploited to characterize the amino functionalized CNTs. Fig. 2 A had shown the IR spectrum of pristine CNTs. The appearance of two fairly weak and broad absorption bands at 3450 cm^{-1} and 1638 cm^{-1} were due to the presence of –OH groups on the surface of the pristine CNTs, which could be the result of the ambient atmospheric moisture bound to the CNTs (Ma et al., 2006). For the IR spectrum of CNT–OH, the increased band at 3443 cm^{-1} suggested that there were more –OH groups on the CNTs surface and the CNTs were expectedly hydroxylated (Song et al., 2009). In the spectrum of CNT–NH_2, the new absorption peaks at 1112 cm^{-1} was ascribed to Si–O–Si vibration, while the band at 686 cm^{-1} could be due to the stretching of Si–C bonds. The aforementioned performances had confirmed the occurrence of amino functionalization of CNTs (Kathi and Rhee, 2008).

XPS spectrums for the CNT–NH_2 were shown in Fig. 2B, with the chemical compositions listed in the table inset. For the pristine CNTs, the binding energy (BE) of ca. 286.1 eV (O 1 s, at%: 3.11) could be attributed to atmospheric moisture (Ramanathan et al., 2005), which was consistent with the IR results mentioned above. For the CNT–OH, a stronger photoemission at a BE of ca. 286.1 eV was displayed and the composition of oxygen increased up to 5.53 at%, which suggested the CNTs was successfully hydroxylated. In the XPS spectrum of CNT–NH_2, two new photoemission peaks appeared at BEs of 102.9 eV (Si 2p, at%: 3.33) and 399.8 eV (N 1 s, at%: 1.90). Besides, the concentration of oxygen increased up to 6.85, which was attributed to the hydrolysis of 3-APTES. The phenomena above indicated the amino functionalization of the CNTs. Additionally, the splitting of the N 1 s peak from one photoemission peak at BEs of 399.8 eV to two peaks at BEs of 399.6 eV (R–NH_2) and BEs of 400.2 eV (C–N, N–H) (see Fig. 2C) indicated that the primary amino group (–NH_2) was chemically bonded to the surface of CNTs.

3.2. Electrochemical behavior of the modified biosensor

The modification process of the biosensor was characterized by electrochemical impedance spectroscopy (EIS). The results were displayed in the supporting information. In Fig. S1, curve a presented a small semicircle domain implying a low electron transfer resistance (R_{et}) about 125Ω on the bare glassy carbon electrode. After the modification of CNT–NH_2, the R_{et} decreased dramatically to about 80Ω (curve b) which could be attributed to the excellent conductivity and larger effective surface area of amino functionalized CNTs. After AChE was modified onto CNT–NH_2/GCE, the EIS presented an apparent increase and the R_{et} was about 1500Ω (curve c), indicating the fact that AChE had been successfully immobilized onto the CNT–NH_2 modified GCE.

3.3. Enzyme immobilization studies

In order to discuss the influence of different functional groups during the enzyme immobilization processes, DPV behaviors of different functionalized CNTs modified biosensors for ATCh were also evaluated. From the Fig. 3A, it could be found that, in the absence of ATCh, no oxidation peaks were observed. In contrast, the peak current increased in different degrees at the four kinds of modified electrodes after the addition of 0.1 mM ATCh, and decreased in the following order: AChE/CNT–NH_2/GCE > AChE/CNT–COOH/GCE > AChE/CNT–OH/GCE > AChE/pristine CNTs/GCE, which could account for the larger amount of immobilized AChE on the surface of CNT–NH_2 with electrostatic interaction as the driven force. To confirm it, the amount of adsorbed enzyme on different functionalized CNTs was studied. The results summarized in Fig. 3B indicated that larger amount of enzymes were preferentially adsorbed on the positively charged CNTs (CNT–NH_2) than the negatively charged ones (CNT–OH and CNT–COOH). Besides, there were more enzymes adsorbed on the functionalized CNTs than the pristine CNTs, possibly owing to that the functionalization of CNTs enhanced the interfacial adhesion between the nanotubes and the enzymes (Tasis et al., 2006).

From Fig. 3B, it was also noted that the peak current of AChE/CNT–NH_2/GCE increased more sharply than the increase of protein amount adsorbed on CNT–NH_2, which suggested that a more favorable orientation could be achieved on the surface of CNT–NH_2 than other kind of functionalized CNTs. For one side, the axis of the dipole moment of AChE is oriented approximately along

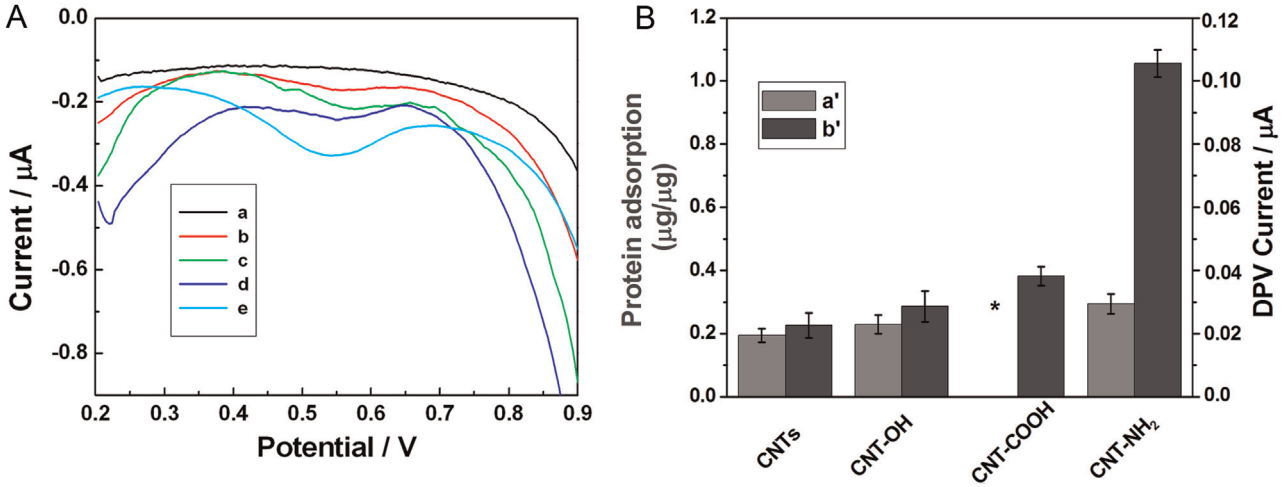

Fig. 3. (A) Differential pulse voltammograms of different modified GCEs (a) AChE/CNT–NH_2/GCE without 0.1 mM ATCh in 0.1 M PBS. (b) AChE/pristine CNTs/GCE, (c) AChE/CNT–OH/GCE, (d) AChE/CNT–COOH/GCE and (e) AChE/CNT–NH_2/GCE within 0.1 mM ATCh in 0.1 M PBS. (B) (a′) The amount of adsorbed protein on the surface of different CNTs, (b′) the absolute value of DPV current to 0.1 mM ATCh at different modified GCEs. Error bars indicated the standard deviations are ranging from 2.2% to 4.9% ($n=3$). *CNT–COOH could not been centrifuged under the speed of 12000 rpm, thus the amount of adsorbed protein on CNT–COOH was not obtained.

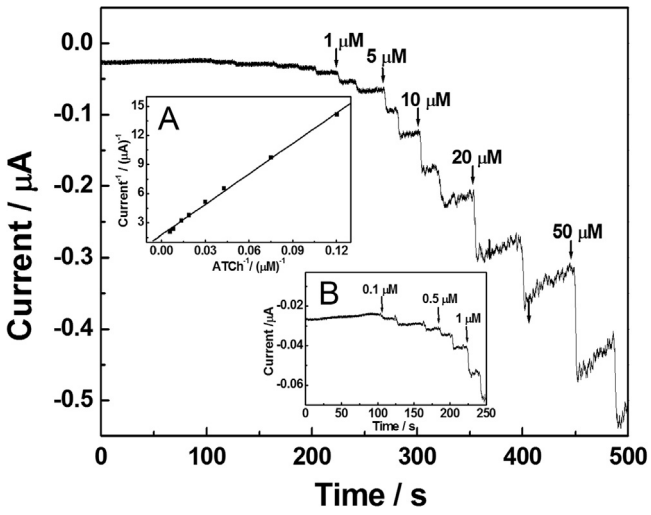

Fig. 4. Amperometric current–time curve of AChE/CNT–NH_2/GC electrode at 0.55 V with successive addition of different concentrations of ATCh into 0.1 M PBS. Inset (A) the Lineweaver–Burk plot of i_s^{-1} versus C^{-1}. Inset (B) the magnified image of the low concentration of ATCh.

with the axis of the active–site gorge, which means the side with the active–site gorge could be predominated negative potential (Dvir et al., 2010; Ripoll et al., 1993). For the other side, it was also reported that there were 6–9 negative charges near the gorge in Electrophorus AChE (Nolte et al., 1980). Therefore, the enzyme could be orderly adsorbed on the CNT–NH_2 and orientated along with the active-site gorge near the surface of CNTs. As the Schematic illustration shown in Fig. 1B, this orientation could reduce the distance between the enzyme active site and the catalytic active site of the electrode surface, inducing faster electron transfer and more efficient reaction.

3.4. Enzyme affinity and catalytic activity to ATCh

Fig. 4 had shown the current–time curve of electrochemical response versus successive addition of different concentrations of ATCh at AChE/CNT–NH_2/GCE, in which the current increased and reached the steady state within 5 s as the addition of ATCh. To value the AChE activity in the enzymatic reaction with ATCh as substrate, Michaelis–Menten constant (K_m) was calculated with Lineweaver–Burk equation (Eq. 1):

$$\frac{1}{i_s} = \frac{K_m}{i_{max}} \times \frac{1}{C} + \frac{1}{i_{max}} \quad (1)$$

where i_s is the steady state current after substrate addition, i_{max} is the maximum current under saturated substrate concentration and C is the concentration of substrate in bulk solution (Wang et al., 2011). The inset (A) of Fig. 4 had shown the linear relationship between i_s^{-1} and C^{-1}, ranging from 8.3 μM to 173.3 μM. According to the previous equation, K_m value had been calculated as 67.4 μM from the slope, which was significantly lower than 131 μM (Zhou et al., 2013) and 202 μM (Wang et al., 2011) reported by literatures. The lower value of K_m suggested that the enzyme displayed higher affinity to ATCh, which could be on account of a favorable orientation of AChE adsorbed on the surface of electrode. Besides, the inset (B) had shown the current–time detection limit of ATCh as low as 0.1 μM, which could convincingly demonstrate that the native catalytic activity of AChE was highly maintained.

3.5. Optimization parameters of the biosensor performance

To get high–performance response of the OPs biosensor, we further optimized the experimental parameters, including the pH value, the concentration of CNT–NH_2 and AChE and the inhibition time of the pesticide. As shown in Fig. S2, pH value of 8.0, 0.5 mg/mL CNT–NH_2, 0.02 mg/mL AChE and 10 min incubation time were chosen as the optimal parameters in the subsequent experiment.

3.6. Interference studies

In order to ensure there was no severe bias issue caused by interferences, the effect of potential interfering substances, such as ascorbic acid, glucose, dopamine, urea and uric acid, had been tested. As shown in Table S1, no observable signal changes were detected among all of these compounds. The results demonstrated that the prepared biosensor possessed good selectivity for the measurement of organophosphorus chemicals.

3.7. Pesticide determination

The DPV responses were discussed before and after exposure to paraoxon for about 10 min. On one side, as shown in Fig. 5A, after

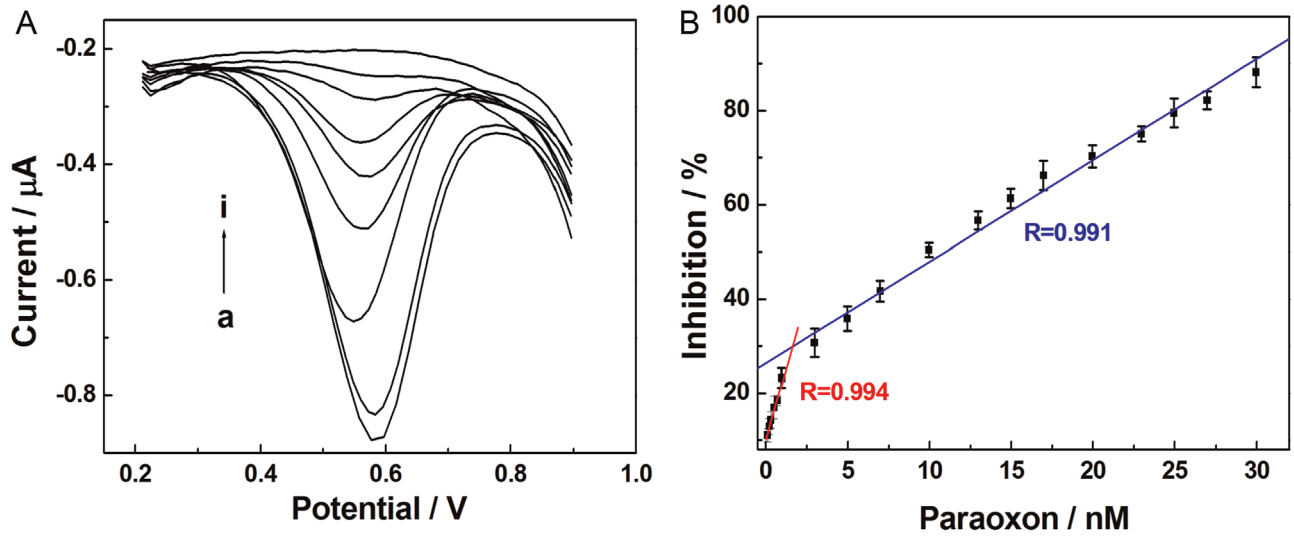

Fig. 5. (A) DPV responses of AChE/CNT–NH_2/GCE in PBS within (a–h) or without (i) 0.4 mM ATCh after incubation with (a) 0, (b) 0.1 nM, (c) 5 nM, (d) 10 nM, (e) 15 nM, (f) 20 nM, (g) 25 nM, (h) 30 nM paraoxon for 10 min. (B) Plots of inhibition current at different concentrations of paraoxon. Error bars indicate the standard deviations ranging from 1.5% to 3.1% (n=5).

Table 1
Correlation of the concentrations of total OPs content in vegetables determined directly by the proposed biosensor with that determined by GC.

Sample	Paraoxon biosensors				GC method		
	Measured value (I %)	Averaged value	Recovery (%)	RSD (%)	Averaged value	Recovery (%)	RSD (%)
Paraoxon[a]		4.78 (μM)	95.6	2.4	4.62 (μM)	92.4	1.8
		9.35 (μM)	93.5	3.1	9.75 (μM)	97.5	2.0
Cabbage	3.70	N/A[b]		5.7	N/A[c]		
Onion	9.25	N/A[b]		4.3	N/A[c]		
Carrot	2.34	N/A[b]		3.7	N/A[c]		
Celery	22.10	Equivalent 0.96 (nM)		2.3	N/A[c]		
Added (5 nM)							
Cabbage	34.98	4.46 (nM)	89.2	9.2	N/A[c]		
Onion	36.84	5.33 (nM)	106.7	5.9	N/A[c]		
Carrot	36.54	5.19 (nM)	103.8	2.9	N/A[c]		

[a] Since the detection limitation of the proposed biosensor was much lower than GC method, the standard paraoxon was diluted before measurement with the biosensor.
[b] The inhibition rate was lower than 10%, so we assumed that OPs were not detected.
[c] Concentration of paraoxon lower than 3.64 μM could not be detected out with GC method.

exposure to different concentrations of paraoxon, the peak currents (curves b–h) dramatically decreased compared with the control (curve a), possibly because paraoxon could attack the serine residue of AChE and inhibit it readily by forming phosphorylated adducts. On the other side, it could be seen from Fig. 5B that the responses were associated with inhibition of the enzyme activity based on the amount of pesticide added. The percentage inhibition of the biosensor could be calculated with Eq. 2:

$$Inhibition\ (\%) = [(I_o - I_i)/I_o] \times 100 \quad (2)$$

where I_o and I_i are the peak currents to 0.4 mM ATCh before and after incubated in different concentrations of paraoxons. As shown in Fig. 5B, the inhibition efficiency of paraoxon was a linear function of its concentration from 0.2 to 1 nM and 1 to 30 nM. The linear equations were *Inhibition* (%)=12.457 C+10.141 from 0.2 nM to 1 nM and *Inhibition* (%)=2.152 C+26.183 from 1 nM to 30 nM (C in nM), with the correlation coefficients of 0.994 and 0.991, respectively. The detection limit was calculated to be 0.08 nM (S/N=3). Comparative studies between the herein biosensor and other published paraoxon biosensors had been conducted. The results summarized in Table S2 had indicated that the OPs biosensor herein had displayed lower detection limit as well as wider linearity ranges than the previous studies (Suprun et al., 2005; Jha and Ramaprabhu, 2010; Ivanov et al., 2011; Joshi et al., 2005; Nayak et al., 2013; Dutta and Puzari, 2014). The good performance could be attributed to the efficient adsorption of AChE on CNT–NH_2 retaining its bioactivity.

3.8. Reproducibility and storage stability

The intra-assay precision was confirmed by evaluating the relative standard deviation (RSD) of sensor response for four continuous measurements with a single fabrication, using 0.1 mM ATCh. Similarly, the inter-assay precision was estimated at six different electrodes. The RSD of intra–assay and inter–assay were found to be 1.5% and 2.4%, respectively. The good reproducibility indicated this method with simple steps displayed a high operability.

The storage stability had been discussed likewise, in which the modified electrodes were stored in a refrigerator at 4 °C, in moist surroundings. As a consequence, the biosensors still remained 95% and 80% response after 7 days and 30 days storage respectively, indicating desirable stability of the biosensor.

3.9. The determination of the real samples

The applicability of the proposed biosensor was assessed by determination of paraoxon in four kinds of vegetable samples. To verify the reliability of this biosensor, the samples were also analyzed by gas chromatography. As was shown in Table 1, the results of the paraoxon content analyzed by the biosensor were in good accordance with those obtained by GC method, demonstrating high accuracy and excellent reliability. The range of the spiked recoveries was from 89.2% to 106.7% and the relative standard deviations were less than 10%. It was also worth recognizing that the average inhibition value of celery samples was about 22.10%, suggesting there were some pesticides residues in these celery samples. After the conversion, the averaged value of pesticide residues in these celery samples was equivalent to 88.1 μg/kg paraoxon, which was eight times more than the maximum residue limits (MRLs) (10 μg/kg) of the particular pesticides established by the European Union (EU) and the governments of its member countries. The above results had adequately demonstrated that the proposed biosensor could be applied for the total OPs detection in real vegetable samples with acceptable accuracy and reliability.

4. Conclusions

Surface functionalized CNTs tailored with amino groups were applied to control the efficient immobilization of AChE onto the surface of glassy carbon electrode and construct a high sensitive pesticide biosensor. Based on this method, the operation process had been simplified while the analysis efficiency and operability had been improved. Consequently, high sensitivity, good stability and reproducibility, wide linear response range and short response time were achieved. Moreover, the proposed electrode had been successfully employed for the direct analysis of vegetable samples. The described technique could be extended to other functionalized nano-materials for their application in developing biosensors.

Acknowledgments

The financial supports from National Basic Research Program of China (973 Program, No. 2015CB352102), Program for New Century Excellent Talents in University (No. NCET-13-0232) and the Fundamental Research Funds for the Central Universities (Huazhong University of Science and Technology, 2013TS010) are greatly

acknowledged. The Center of Analysis and Testing of Huazhong University of Science and Technology is thanked for its help in XPS and IR.

Appendix A. Supplementary material

Supplementary data associated with this article can be found in the online version at http://dx.doi.org/10.1016/j.bios.2015.01.005.

References

Choi, J.W., Kim, Y.K., Lee, I.H., Min, J.H., Lee, W.H., 2001. Biosens. Bioelectron. 16 (9-12), 937–943.
Dutta, R.R., Puzari, P., 2014. Biosens. Bioelectron. 52, 166–172.
Dvir, H., Silman, I., Harel, M., Rosenberry, T.L., Sussman, J.L., 2010. Chem.–Biol. Interact. 187 (1–3), 10–22.
Ganesana, M., Istarnboulie, G., Marty, J.-L., Noguer, T., Andreescu, S., 2011. Biosens. Bioelectron. 30 (1), 43–48.
Gessner, A., Lieske, A., Paulke, B.R., Müller, R.H., 2003. J. Biomed. Mater. Res. A 65 (3), 319–326.
Hoshino, Y., Koide, H., Urakami, T., Kanazawa, H., Kodama, T., Oku, N., Shea, K.J., 2010. J. Am. Chem. Soc. 132 (19), 6644–6645.
Ivanov, A., Younusov, R., Evtugyn, G., Arduini, F., Moscone, D., Palleschi, G., 2011. Talanta 85 (1), 216–221.
Jha, N., Ramaprabhu, S., 2010. Nanoscale 2 (5), 806–810.
Joshi, K.A., Tang, J., Haddon, R., Wang, J., Chen, W., Mulchandani, A., 2005. Electroanalysis 17 (1), 54–58.
Kathi, J., Rhee, K., 2008. J. Mater. Sci. 43, 33–37.
Kim, S.N., Rusling, J.F., Papadimitrakopoulos, F., 2007. Adv. Mater. 19 (20), 3214–3228.
Lai, G.-S., Zhang, H.-L., Han, D.-Y., 2009. Microchim. Acta 165 (1–2), 159–165.
Li, C., Wang, C., Wang, C., Hu, S., 2006. Sens. Actuat. B-Chem 117 (1), 166–171.
Liu, G., Lin, Y., 2006. Anal. Chem. 78 (3), 835–843.
Liu, G., Riechers, S.L., Mellen, M.C., Lin, Y., 2005. Electrochem. Commun. 7 (11), 1163–1169.
Ma, P.C., Kim, J.-K., Tang, B.Z., 2006. Carbon 44 (15), 3232–3238.
Meder, F., Daberkow, T., Treccani, L., Wilhelm, M., Schowalter, M., Rosenauer, A., Madler, L., Rezwan, K., 2012. Acta Biomater. 8 (3), 1221–1229.
Meder, F., Hintz, H., Koehler, Y., Schmidt, M.M., Treccani, L., Dringen, R., Rezwan, K., 2013a. J. Am. Chem. Soc. 135 (16), 6307–6316.
Meder, F., Kaur, S., Treccani, L., Rezwan, K., 2013b. Langmuir 29 (40), 12502–12510.
Monopoli, M.P., Aberg, C., Salvati, A., Dawson, K.A., 2012. Nat. Nanotechnol. 7 (12), 779–786.
Nayak, P., Anbarasan, B., Ramaprabhu, S., 2013. J. Phys. Chem. C 117 (25), 13202–13209.
Nolte, H.-J., Rosenberry, T.L., Neumann, E., 1980. Biochemistry 19 (16), 3705–3711.
Ramanathan, T., Fisher, F.T., Ruoff, R.S., Brinson, L.C., 2005. Chem. Mater. 17 (6), 1290–1295.
Ripoll, D.R., Faerman, C.H., Axelsen, P.H., Silman, I., Sussman, J.L., 1993. Proc. Natl. Acad. Sci. USA 90 (11), 5128–5132.
Song, P., Shen, Y., Du, B., Guo, Z., Fang, Z., 2009. Nanoscale 1 (1), 118–121.
Sotiropoulou, S., Fournier, D., Chaniotakis, N.A., 2005. Biosens. Bioelectron. 20 (11), 2347–2352.
Suprun, E., Evtugyn, G., Budnikov, H., Ricci, F., Moscone, D., Palleschi, G., 2005. Anal. Bioanal. Chem. 383 (4), 597–604.
Tasis, D., Tagmatarchis, N., Bianco, A., Prato, M., 2006. Chem. Rev. 106 (3), 1105–1136.
Tzavalas, S., Drakonakis, V., Mouzakis, D.E., Fischer, D., Gregoriou, V.G., 2006. Macromolecules 39 (26), 9150–9156.
Wang, Y., Zhang, S., Du, D., Shao, Y., Li, Z., Wang, J., Engelhard, M.H., Li, J., Lin, Y., 2011. J. Mater. Chem. 21 (14), 5319–5325.
Zhang, S., Wang, N., Yu, H., Niu, Y., Sun, C., 2005. Bioelectrochemistry 67 (1), 15–22.
Zhou, Q., Yang, L., Wang, G., Yang, Y., 2013. Biosens. Bioelectron. 49, 25–31.
Zou, Y., Xiang, C., Sun, L.-X., Xu, F., 2008. Biosens. Bioelectron. 23 (7), 1010–1016.